Polymer Testing 154 (2026) 109055

Contents lists available at ScienceDirect

Polymer Testing

journal homepage: www.elsevier.com/locate/polytest

Mode-II interlaminar damage in carbon/epoxy composites fabricated via hot-press and vacuum-bagging techniques

K.J. Wong [a,*], H.A. Israr [b], T. Dickhut [c], S.S.R. Koloor [c,**], M.N. Tamin [b]

[a] Department of Mechanical, Materials and Manufacturing Engineering, Faculty of Science and Engineering, University of Nottingham Malaysia, Jalan Broga, 43500, Semenyih, Selangor, Malaysia
[b] Faculty of Mechanical Engineering, Universiti Teknologi Malaysia, UTM Skudai, 81310, Johor, Malaysia
[c] Composite Materials and Engineering Mechanics, Institute of Aeronautical Engineering, Faculty of Mechanical Engineering, Universität der Bundeswehr München, Werner-Heisenberg-Weg 39, Neubiberg, 85579, Munich, Germany

ARTICLE INFO

Keywords:
Carbon/epoxy composites
Mode II delamination
Fabrication techniques
Scanning electron microscopy
Cohesive zone model

ABSTRACT

Understanding mode II delamination in thermoset composites remains incomplete, particularly when fabrication-induced variability affects interfacial characteristics and fracture performance. This research fabricates unidirectional carbon/epoxy prepregs via hot-press (HP) and vacuum-bagging (VB) techniques and evaluates their interlaminar fracture behaviour through End-Notched Flexure (ENF) testing. Results indicate that the mode II fracture toughness (G_{IIC}) of VB specimens (1387 N/m) is approximately 33 % lower than that of HP specimens (2058 N/m). Scanning electron microscopy (SEM) reveals reduced shear cusp density and matrix cracking in VB specimens. Delamination behaviour is simulated using a symmetric Trapezoidal Traction-Separation Law (TTSL) with pseudo-plasticity parameter $\Gamma = 0.99$, which, aside from differing G_{IIC} values, employs a consistent set of cohesive parameters (interface stiffness $k_{IIC} = 4.5 \times 10^5$ MPa/mm and interface strength $t_{u,II} = 100$ MPa) to accurately reproduce the force-displacement response in both fabrication methods. A higher G_{IIC} value corresponds to greater crack extension (da) in simulated damage profiles, with $da = 2.9$ mm and 2.5 mm in HP and VB specimens, respectively. The numerical model is further validated using VB specimens with varied initial crack lengths, consistently producing reliable results. These outcomes validate the proposed unified framework, with all cohesive parameters, except for the experimentally determined G_{IIC}, which are kept constant (Γ, k_{IIC} and $t_{u,II}$). This approach significantly reduces the need for extensive parametric studies in numerical simulations, thereby improving efficiency and consistency.

1. Introduction

Autoclave (AC) processing is widely used to fabricate high-quality composite laminates [1]. However, out-of-autoclave (OOA) techniques, such as vacuum-bagging (VB), have gained traction due to lower equipment requirements [2] and fewer size constraints [3]. Ensuring mechanical equivalence between AC- and OOA-fabricated composites is essential for broader industrial adoption.

Several studies have shown that the composites fabricated using AC and OOA methods exhibit comparable mechanical properties. For instance, unnotched compressive strength, notched compressive strength, and short beam shear strength were found to be similar for both fabrication methods when the prepregs were processed within a few days of ambient exposure. [4]. Likewise, woven carbon/epoxy composites cured using the repair-clave (RC) method demonstrated equivalent flexural and compressive performance [1]. Comparable interlaminar shear strength (ILSS) was also observed in single scarf repairs of woven glass/epoxy composites cured via AC and vacuum-bagging (VB) methods [2]. Furthermore, plain weave glass fabric reinforced epoxy composites cured using AC, oven (OV), single (SVB), and double (DVB) vacuum bagging techniques showed minimal differences in normalised tensile modulus and tensile strength [5]. However, AC-cured samples exhibited superior normalised interlaminar shear stiffness compared to the other methods, and both AC and OV curing yielded higher ILSS than SVB and DVB. In contrast, for woven E-glass/lycal epoxy composites, the vacuum infusion (VI) method

* Corresponding author.
** Corresponding author.
E-mail addresses: kingjye.wong@nottingham.edu.my (K.J. Wong), seyed.rahimian@unibw.de (S.S.R. Koloor).

https://doi.org/10.1016/j.polymertesting.2025.109055
Received 27 August 2025; Received in revised form 6 November 2025; Accepted 20 November 2025
Available online 20 November 2025

outperformed VB and hand lay-up (HL) techniques in terms of compressive and shear properties [6]. Based on the aforementioned literature, it is commonly observed that AC and OOA fabrication methods can yield comparable mechanical properties. However, the mechanical performance is influenced not only by the fabrication technique but also by the specific material system used. This highlights the importance of considering both factors when evaluating or comparing composite performance.

Delamination, or interface debonding between two materials in an integrated structural system [7], often attributed to the inherently low interlaminar strength of composite laminates, is widely recognised as an early failure mode [8,9]. Delamination is often characterised using fracture toughness properties, indicating the energy require for interface damage evolution and crack growth [10]. In terms of mode I fracture toughness (G_{IC}), AC-fabricated laminates, whether produced via hand lay-up or fibre placement, showed consistent values with negligible resistance curve (R-curve) effects [4]. Conversely, OOA-fabricated composites exhibited pronounced R-curve behaviour, likely due to weaker fibre/matrix interfacial bonding. More recently, it was found that the G_{IC} values were similar for hot-press (HP) and vacuum-bagging (VB) specimens, although VB samples displayed significant fibre bridging [11].

The Cohesive Zone Model (CZM) is commonly recognised for its effectiveness in replicating delamination phenomena in laminated composites and bonded joints [12,13]. Utilising finite element techniques, CZM facilitates in-depth analysis of stress fields, initiation of material degradation, and crack progression, serving as a viable substitute for intricate experimental setups. The reliability of CZM outcomes is closely tied to the formulation of the traction-separation law (TSL) applied [14–16]. Among these, the bilinear TSL (BTSL) is frequently used due to its straightforward implementation and suitability for simulating brittle and semi-ductile materials [17]. Nevertheless, BTSL may fall short when used with ductile adhesives, as it does not fully capture their mechanical response [14]. In such scenarios, the trapezoidal TSL (TTSL) offers a more accurate representation, especially for interfaces that exhibit elastic-plastic or non-linear fracture characteristics [18–22]. According to May et al. [23], extending the plateau region in TTSL enhances its ability to model materials with greater ductility.

TTSL has been successfully applied in various studies to model mode II delamination, including investigations on unidirectional glass/epoxy composites [24], unidirectional carbon fibre composites bonded adhesive joints [25], glass/epoxy composite bonded nano-alumina powder-reinforced adhesive joints [26], and fibre-metal laminates (FMLs) with doubler and splice configurations [19,20]. These findings underscore the adaptability of TTSL across a wide range of materials and loading conditions. Prior research has demonstrated its effectiveness in modelling mode II delamination for both dry and moisture-exposed specimens [27], suggesting its suitability for composites fabricated using different techniques.

Based on the aforementioned literature review, it is evident that studies on the delamination behaviour of composite laminates fabricated using different methods remain limited. While mode I delamination is more commonly investigated due to its lower fracture toughness compared to mode II [28–38], mode II delamination is equally important. This is because transverse loading on composite structures typically induces bending, which in turn generates interlaminar shear stresses that can lead to mode II delamination. In aerospace applications, such bending loads are frequently encountered in components such as the fuselage and stabilisers [38]. Although mode II delamination has been extensively studied by various researchers [27,39–47], there is a lack of comparative studies focusing on the influence of fabrication methods. Moreover, in practical scenarios such as aircraft composite repair, VB is often preferred over autoclave curing due to spatial constraints that make AC use impractical [2]. These considerations form the basis and motivation for the current research.

A unified framework for simulating mode II interface delamination process in laminated composites, fabricated by different techniques is proposed in this study. In this respect, mode II delamination behaviour of unidirectional carbon/epoxy laminates fabricated via HP and VB methods was examined through experimental and numerical approaches. Mode II fracture toughness (G_{IIC}) was quantified, and delaminated surfaces were analysed using scanning electron microscopy. The CZM approach incorporating TTSL with varying pseudo-plasticity parameters (Γ) was employed to simulate force-displacement responses and crack growth profiles. The simulation methodology was further validated using VB specimens with different initial crack lengths. This could significantly reduce the amount of experimental works and parametric studies in numerical simulations.

2. Materials and methods

The composite material utilised was T600 S/R368-1 unidirectional carbon/epoxy prepreg from Structil. The prepreg features an areal density of 170 g/m^2, a fibre volume fraction of approximately 59 ± 2 %, and a nominal ply thickness of 0.2 mm. A unidirectional carbon/epoxy composite panel comprising 16 layers and measuring 400 × 400 × 3.2 mm^3 was produced using both HP and VB methods (see Fig. 1). Each layer of prepreg was carefully hand-laid and consolidated using a roller to eliminate any air bubbles trapped between the layers. To create pre-cracks, a 15 μm-thick Teflon insert, 70 mm wide, was placed at the mid-thickness along both edges of each panel.

During the HP process, the panel was cured under a pressure of 5 bar, whereas the VB method involved sealing the prepregs in a vacuum bag and applying vacuum pressure. Both curing processes were carried out at a peak temperature of 125 °C for a total of 155 min, following the curing cycle illustrated in Fig. 2. The resulting composite plates featured a stacking sequence of [0_8//0_8], where "//" indicates the placement of the Teflon insert. Upon completion, the edges of the composite plates were trimmed using an abrasive blade with coolant to ensure clean and precise finishes. For mode II End-Notched Flexure (ENF) testing, specimens were cut to a width of 20 mm. To protect the crack tip during cutting, the uncut section of the composite plate was covered with a rigid steel plate and securely clamped. Fig. 3 shows the ENF test setup, with an initial crack length (a_o) of 25 mm introduced in both specimen types. Testing was performed in displacement-controlled mode using a universal testing machine equipped with a 5 kN load cell, operating at a crosshead speed of 1 mm/min. A minimum of five specimens were tested for each fabrication technique. Prior to scanning electron microscopy (SEM) imaging, the delaminated surfaces were gold-coated using a 134 Bio-Rad Polaron Division coater, and micrographs were captured with a Philips XL40 microscope.

3. Data reduction scheme

The mode II fracture toughness (G_{IIC}) was calculated using Irwin-Kies [48] Equation:

$$G_{IIC} = \frac{P_C^2}{2B}\left(\frac{dC}{da}\right) \tag{1}$$

where P_C represents the critical load, B is the specimen width, C denotes the compliance, and a is the crack length. The compliance was modelled using a calibration equation as described in Ref. [49]:

$$C = C_2 a^3 + C_1 \tag{2}$$

where C_2 and C_1 are constants obtained by fitting a plot of C versus a^3. By substituting the derivative of Eq. (2) into Eq. (1), the expression for G_{IIC} is obtained:

$$G_{IIC} = \frac{P_C^2}{2B} 3C_2 a^2 \tag{3}$$

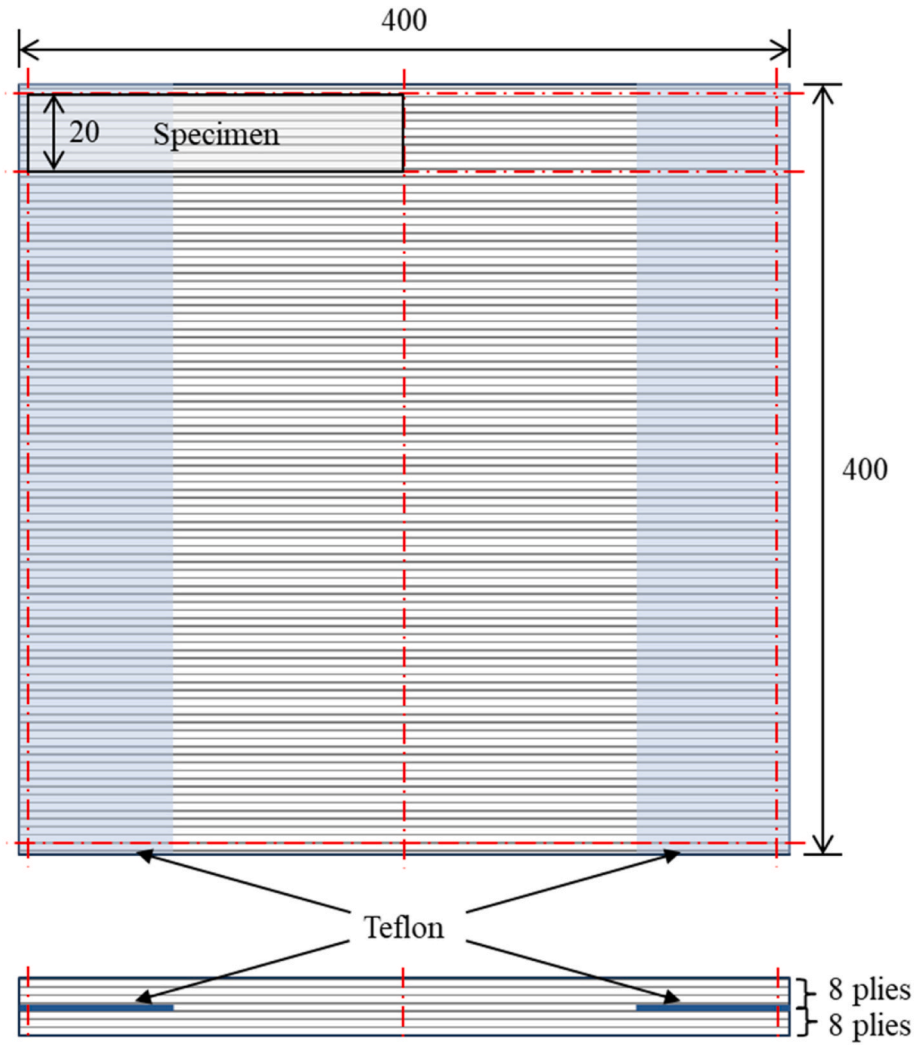

Fig. 1. Schematic illustration of the composite plate layup and specimen preparation process. All dimensions are given in millimetres (mm).

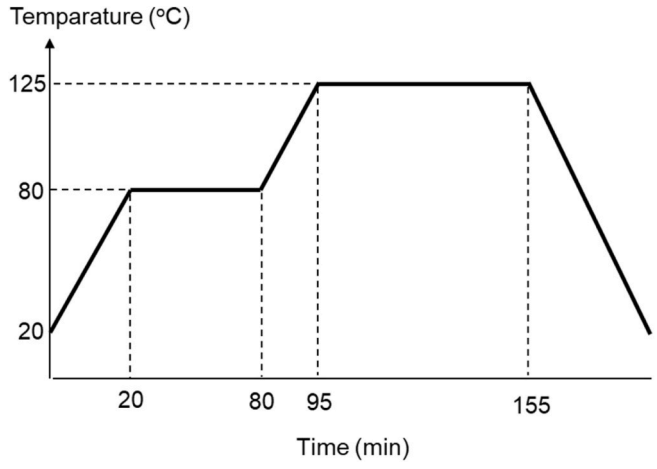

Fig. 2. Curing cycle applied to the carbon/epoxy composites in this study.

4. Trapezoidal Traction-Separation Law

Fig. 4 illustrates the idealised mode II Trapezoidal Traction-Separation Law (TTSL). In the initial phase, the shear traction (t_{II}) increases linearly with the relative displacement (δ_{II}), with the gradient of this segment representing the stiffness of the mode II interface (k_{II}). When the traction reaches the interface strength ($t_{u,II}$), corresponding to the separation $\delta_{o,II}$, damage initiation occurs. As δ_{II} continues to increase, the traction remains constant, representing the interface's plastic response. The point $\delta_{p,II}$ marks the second inflection in the trapezoidal curve. Following the plateau region, the shear traction gradually declines in a linear fashion, culminating in total separation at $\delta_{f,II}$. It is important to note that setting the pseudo-plasticity parameter $\Gamma = 0$ transforms the model into bilinear traction-separation law (BTSL).

The mode II fracture toughness (G_{IIC}), which represents the trapezoidal area, is obtained through experimental procedures. Meanwhile, the mode II penalty stiffness (k_{II}) is set at 4.5×10^5 MPa/mm, and the mode II interface strength ($t_{u,II}$) is chosen to be 100 MPa, based on the methodology outlined in a previous study involving the same material [27]. In summary, k_{II} was determined using:

$$k_{II} = \frac{E_m}{h_{ce}} \tag{4}$$

where the Young's modulus of the epoxy resin, denoted as E_m, is 4.5 GPa, while h_{ce} represents the thickness of the cohesive element, set at 10 μm. Additionally, the value of $t_{u,II}$ was determined through a parametric study over a range of 60–100 MPa. A value of 100 MPa was selected as it yielded the closest peak force in comparison to the experimental results [27]. These three parameters are used to calculate $\delta_{o,II}$, $\delta_{p,II}$, and $\delta_{f,II}$, as explained below.

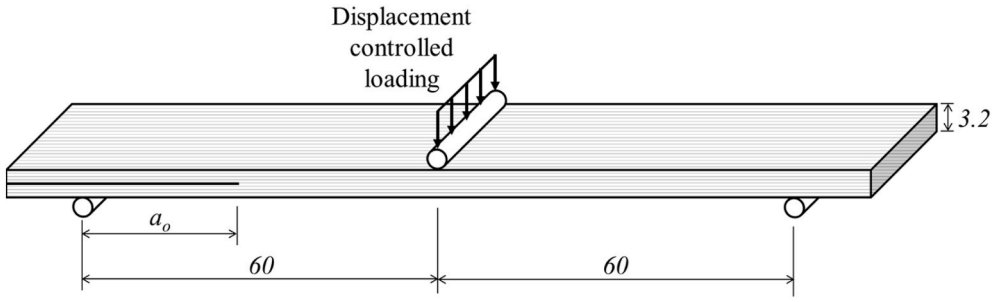

Fig. 3. Setup diagram for End-Notched Flexure test.

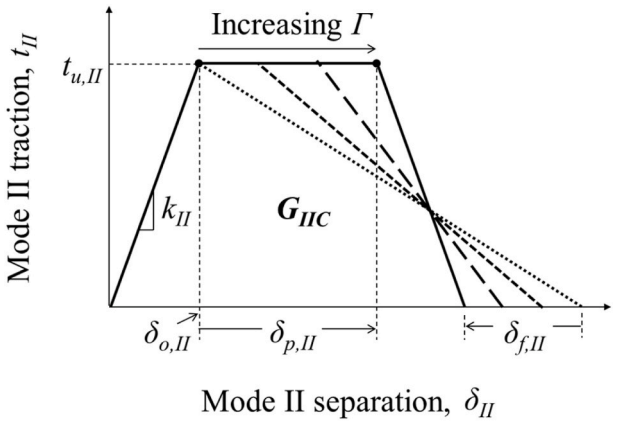

Fig. 4. Trapezoidal traction-separation response under mode II loading.

From Fig. 4, the following observations can be made:

$$\delta_{o,II} = \frac{t_{u,II}}{k_{II}} \tag{5}$$

The pseudo-plasticity parameter, denoted as Γ, is defined as the ratio of the area under the plateau region to the total area beneath the traction–separation curve [23]:

$$\Gamma = \frac{\textit{Area under plateau region}}{\textit{Total area}} = \frac{\left(\delta_{p,II} - \delta_{o,II}\right) t_{u,II}}{G_{IIC}}$$

$$\delta_{p,II} = \delta_{o,II} + \Gamma \frac{G_{IIC}}{t_{u,II}} \tag{6}$$

As illustrated in Fig. 4, an increase in Γ indicates a higher degree of plasticity and a corresponding decrease in $\delta_{f,II}$. In simpler terms, greater plasticity results in a faster reduction of traction within the softening zone. Additionally, it is important to note that several simulations were conducted to evaluate the effect of Γ, using values of 0, 0.2, 0.4, 0.6, 0.8, and 0.99. Specifically, $\Gamma = 0$ represents BTSL, while $\Gamma = 0.99$ reflects a condition where the slope of the softening region equals k_{II}.

Summing the area under the trapezium, the G_{IIC} is expressed as:

$$\begin{aligned} G_{IIC} &= \frac{1}{2} t_{u,II}\delta_{o,II} + t_{u,II}\left(\delta_{p,II} - \delta_{o,II}\right) + \frac{1}{2} t_{u,II}\left(\delta_{f,II} - \delta_{p,II}\right) \\ &= \frac{1}{2} t_{u,II}\delta_{o,II} + t_{u,II}\delta_{p,II} - t_{u,II}\delta_{o,II} + \frac{1}{2} t_{u,II}\delta_{f,II} - \frac{1}{2} t_{u,II}\delta_{p,II} \\ &= -\frac{1}{2} t_{u,II}\delta_{o,II} + \frac{1}{2} t_{u,II}\delta_{p,II} + \frac{1}{2} t_{u,II}\delta_{f,II} \\ &= \frac{1}{2} t_{u,II}\left(\delta_{f,II} + \delta_{p,II} - \delta_{o,II}\right) \end{aligned} \tag{7}$$

The value of $\delta_{f,II}$ can therefore be calculated using:

$$\delta_{f,II} = \frac{2G_{IIC}}{t_{u,II}} + \delta_{o,II} - \delta_{p,II} \tag{8}$$

At each increment of δ_{II}, the damage parameter (D) is computed and subsequently incorporated into the finite element model.

$$D = \begin{cases} 1 - \dfrac{\delta_{o,II}}{\delta_{II}} & \textit{for} \quad \delta_{o,II} \le \delta_{II} \le \delta_{p,II} \\ 1 - \dfrac{\delta_{o,II}\left(\delta_{f,II} - \delta_{II}\right)}{\delta_{II}\left(\delta_{f,II} - \delta_{p,II}\right)} & \textit{for} \quad \delta_{p,II} \le \delta_{II} \le \delta_{f,II} \end{cases} \tag{9}$$

5. Finite element modelling

Fig. 5 presents the finite element representation of the ENF sample. As shown in Fig. 5(a), the laminated composite was modelled using SC8R continuum shell elements, while the interfacial region at the mid-thickness location was defined using COH3D8 cohesive elements with a thickness of 10 μm. The contact surface between the upper and lower arms was modelled using a surface-to-surface contact formulation, incorporating finite sliding and frictionless tangential behaviour. The laminate's thickness (z-axis) was discretised into four elements. A roller support was imposed at the bottom-left corner, and a pinned support was used at the right end as boundary conditions. To replicate the experimental conditions, a vertical displacement was applied at the centre of the specimen to simulate loading.

In the longitudinal direction, Fig. 5(b) shows that the delamination zone was finely meshed with 0.1 mm elements, while regions outside this zone used a coarser mesh of 2 mm. Across the width, the mesh size was set to 0.5 mm. This modelling approach has been validated to yield accurate simulation results, as demonstrated in previous research [27]. The lamina properties of the unidirectional carbon/epoxy composite used are listed in Table 1. A previous study demonstrated that the same composite material, when fabricated using both HP and VB techniques, exhibited identical mechanical properties [11]. The finite element simulations were performed using Abaqus FE analysis software.

6. Results and discussion

6.1. Force-displacement curves

The solid line in Fig. 6 represents the typical experimental force-displacement responses obtained from the ENF tests. In both Fig. 6(a) and (b) – corresponding to specimens produced via HP and VB, respectively – the force initially increases linearly with displacement, indicating elastic behaviour. Upon reaching the peak force, a noticeable drop occurs, signifying a sudden crack propagation along the interface of the specimen. It is worth noting that the average slope for HP specimens is 134.58 N/mm, while that for VB specimens is 135.23 N/mm. This negligible difference partially validates that the elastic properties of specimens fabricated using both methods are comparable.

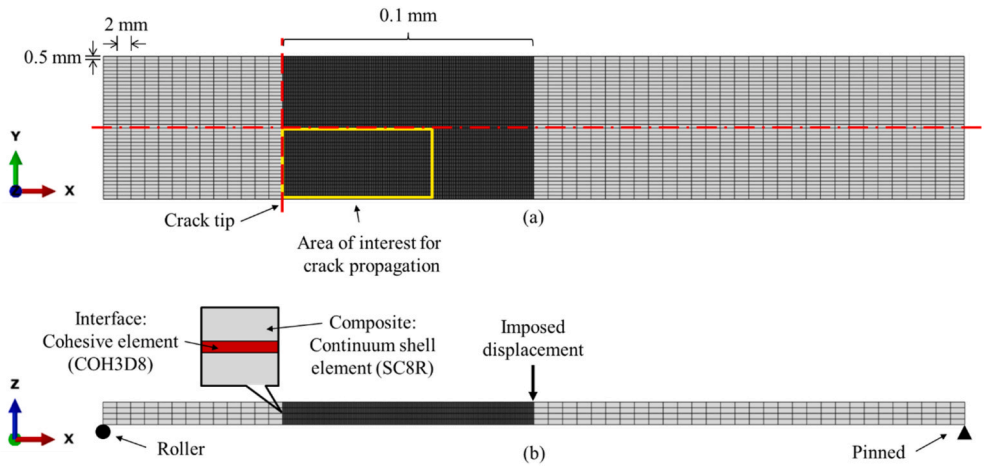

Fig. 5. Finite element model of mode II delamination in composite under ENF loading: (a) top, and (b) side view.

Table 1
Unidirectional carbon/epoxy composite lamina specifications [27].

E_{11} (GPa)	E_{22} (GPa)	G_{12} (GPa)	G_{13} (GPa)	G_{23} (GPa)	ν_{12}
103.0	*6.7*	*2.7*	*2.7*	*2.5*	*0.34*

6.2. Compliance plot

Fig. 7 presents the compliance curves for ENF specimens tested with varying initial crack lengths. For specimens fabricated via HP and VB, the optimal fitting parameters k are 5.37×10^{-8} and 4.18×10^{-8}, respectively, as derived from Eq. (3). The corresponding n values are 7.13×10^{-3} and 6.63×10^{-3}. Both compliance plots exhibit a high degree of correlation, with R^2 values approaching unity, indicating excellent fit quality.

6.3. Mode II fracture toughness

As illustrated in Fig. 8, the average mode II fracture toughness (G_{IIC}) of the unidirectional carbon-epoxy composites, calculated using Eq. (3), is 2058.27 N/m for the HP specimens and 1387.19 N/m for the VB specimens. This indicates that the G_{IIC} value for VB specimens is about 33 % lower than that of the HP specimens. The error bars represent the standard deviation associated with each fabrication method, measured at 160.86 N/m for HP and 221.65 N/m for VB. The values in parentheses represent the coefficient of variation (C.V) in percentage for each fabrication method. Values of 7.8 % for HP and 16.0 % for VB indicate reliable repeatability of the tests. Furthermore, the lower C.V observed in the HP method suggests a more consistent and uniform quality in the fabricated specimens.

Compared to mode I delamination of the same material fabricated using HP and VB methods [11], mode II delamination exhibits distinct behaviour. Firstly, the mode I fracture toughness (G_{IC}) was found to be consistent across both fabrication methods. However, the G_{IIC} for VB specimens was approximately 33 % lower than of HP specimens. Secondly, a significant R-curve was observed in mode I VB specimens due to fibre bridging, whereas HP specimens exhibited a negligible R-curve. In contrast, mode II delamination in both HP and VB specimens was characterised by a sudden crack jump, evidenced by an abrupt drop in force following the peak load. Consequently, for mode I delamination, a bilinear-exponential traction–separation law (BETSL) was employed to simulate delamination growth in VB specimens, while a simpler bilinear traction–separation law (BTSL) was sufficient for HP specimens. For mode II delamination, due to the absence of a significant R-curve in both cases, a trapezoidal traction–separation law (TTSL) was adequate to describe the delamination behaviour. Additionally, it is noteworthy that for both fabrication methods, G_{IC} consistently remained lower than G_{IIC}. Given the complexity of loading conditions in real-world applications, future work should consider extending the study to mixed-mode delamination.

6.4. Fractographic analysis

Fig. 9 shows SEM images comparing the delaminated surfaces of HP and VB specimens. Prominent features such as shear cusps and matrix cracking are evident in both ENF specimens, consistent with observations reported in shear-mode delamination studies by other researchers [46]. Shear cusps are indicative of cohesive failure within the matrix [38]. Similar features have also been observed in the adhesive matrix of carbon fibre/polyether-ketone-ketone (CF/PEKK) composites bonded with Scotch-Weld AF 163–2 K structural adhesive film, patricularly after exposure to cyclic hygrothermal loading, attributed to plasticisation effects [50]. However, the shear cusps in the hot-press specimens appear shorter and more densely distributed, which may have contributed to greater energy dissipation and, consequently, a higher fracture toughness [51]. In a previous study on mode I delamination of the same carbon/epoxy composite, SEM revealed that the VB specimen exhibited weaker fibre/matrix interfacial bonding, which contributed to fibre bridging during delamination propagation [11]. SEM observations from both mode I and mode II delamination tests consistently indicate that the interface quality in HP specimens is superiour to that in VB specimens. This improvement is likely due to the direct pressure applied during HP fabrication, which may compress the laminate more effectively than the vacuum pressure used in VP laminate. As a result, the resin is distributed more uniformly, leading to a thinner resin-rich area [6]. A reduced resin-rich region can minimise stress concentration and enhance fibre/matrix interfacial bonding.

Sutter et al. [4] compared mode I delamination behaviour between AC-cured IM7/977–3 and OOA-cured IM7/MTM45-1 carbon/epoxy composites. SEM analysis of the fractured surface of the IM7/977-3 specimen revealed extensive matrix remnants on the fibres, indicating strong fibre/matrix interfacial bonding. In constrast, the IM7/MTM45-1 specimen exhibited a significant number of bare fibres, suggesting weaker interfacial bonding between the fibre and matrix. A greater number of bare fibers are observed on the fractured interface of VB sample, as shown in Fig. 9(b). This suggests that a weaker fiber/matrix interfacial bonding following the VB fabrication process compared to HP process. However, the preceding discussion is limited to a qualitative assessment of the SEM observations. While qualitative analysis provides valuable insignts, it primarily serves to support comparative evaluations of damage mechanisms in specimens fabricated using different methods.

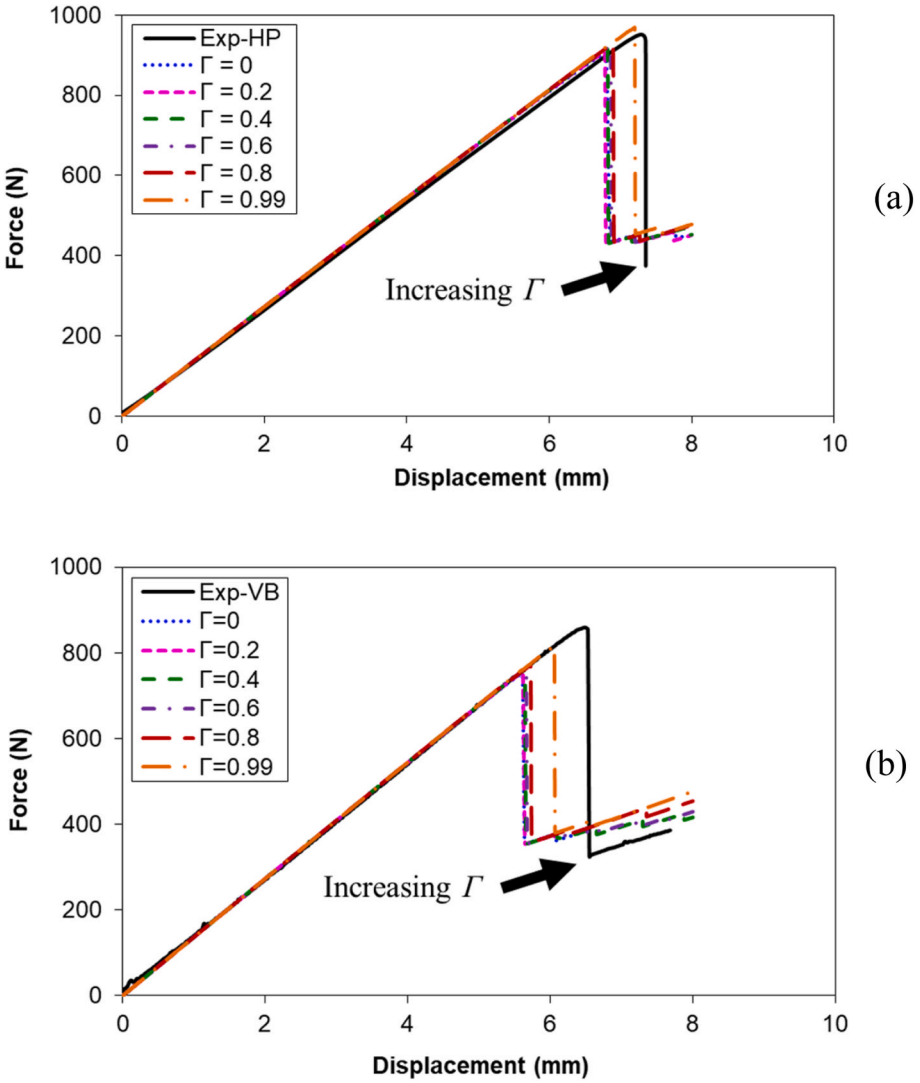

Fig. 6. Mode II delamination force-displacement curves: experimental vs. numerical for (a) hot-press and (b) vacuum-bagging composites.

To enhance the robustness of these findings, quantitative image analysisi techniques such as those available in ImageJ and MATLAB could be employed in future work [52]. These tools would enable more objective and reproducible measurements of fracture surface features, thereby strengthening the interpretation of interfacial failure characteristics.

According to Centea et al. [3], vacuum application removes entrapped air, thereby reducing macro-void formation and compacting the fibre bed. As the temperature increases, the resin gradually infiltrates the fibre network and bonds the fibres together. Ideally, the cured composite laminate should be void-free, however, in practice, flow-induced voids may still be present due to the incomplete resin impregnation of dry areas before gelation. Fig. 10(a) presents a schematic diagram of the hand-laid unidirectional carbon/epoxy prepregs, while Fig. 10(b) illustrates the composite laminate after curing under pressure and temperature. Since both HP and VB laminates were fabricated using the same curing cycle, they are theoretically expected to exhibit similar elastic properties. This observation aligns with findings from a previous study on the same material fabricated using identical methods [11]. Similarly, Dewangan and Chakladar [5] reported that the normalised tensile modulus of plain weave glass fabric reinforced epoxy composites remained consistent across specimens fabricated using vacuum pump, double vacuum-bagging, oven curing and autoclave curing.

Nevertheless, resin flow at the crack tip may differ due to variations in pressure application methods – direct application in HP versus vacuum pressure in VB – which can lead to differences in interface quality and consequently, distinct delamination behaviour. As illustrated in Fig. 11, variations in the resin-rich region is believed to influence the fracture process zone (FPZ), thereby affecting the delamination response [53]. This variation is thought to alter the initial conditions at the crack tip, which significantly affects the G_{IIC} of laminates produced by different fabrication methods.

6.5. Determination of cohesive parameters

Fig. 6 depicts how variations in Γ influence the simulated force-displacement profiles for specimens produced via HP and VB methods. For both fabrication methods, increasing Γ results in a modest elevation in the simulated peak force, while the numerical stiffness remains largely unaffected. The simulation results show the closest agreement with experimental data at $\Gamma = 0.99$, with deviations of 2 % for HP specimens and 5 % for VB specimens. This underscores the importance of selecting an appropriate Γ value when applying the TTSL to achieve accurate simulation outcomes. Furthermore, the experimental and numerical slopes for both fabrication methods show good agreement, further supporting the use of same elastic properties for both fabrication methods listed in Table 1.

Importantly, when comparing HP and VB specimens, the cohesive zone model is independent of $t_{u,II}$, k_{II}, and Γ – with the only variation

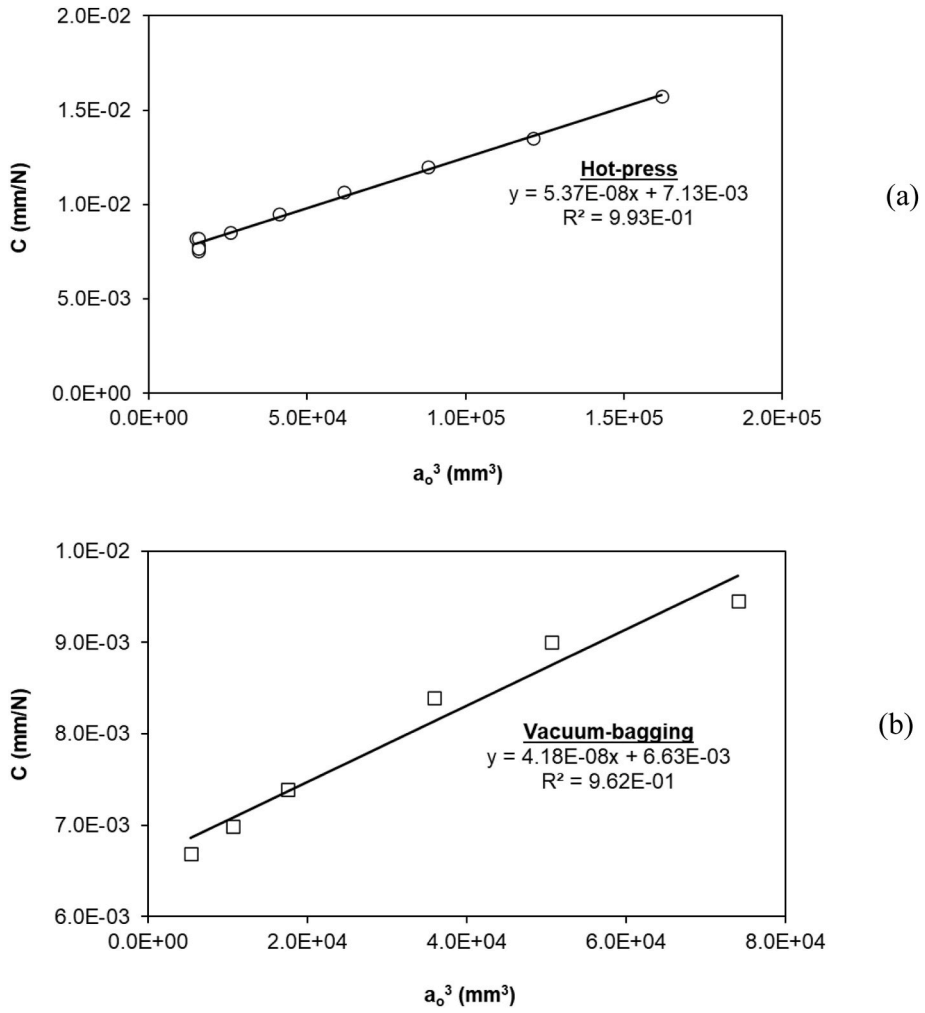

Fig. 7. Mode II compliance plots for UD carbon/epoxy: (a) hot-press, (b) vacuum-bagging, at different crack lengths.

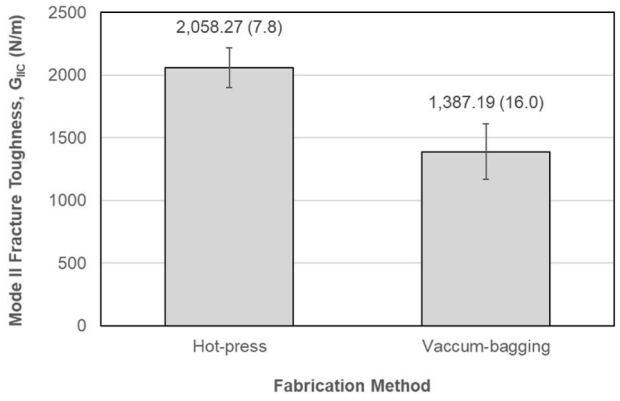

Fig. 8. Influence of processing method on mode II fracture toughness in UD carbon/epoxy laminates.

being the G_{IIC} value. This finding is significant, as it simplifies the simulation process for the same material fabricated using different techniques, reducing the need for extensive parametric studies. Table 2 summarises the cohesive parameters used in the mode II delamination simulations for both HP and VP specimens.

From the force-displacement data in Fig. 6, the damage profile at the time of peak force is extracted. To take advantage of specimen symmetry, analysis was limited to one half of the width within the delamination region of interest, as shown in yellow in Fig. 5(a). In Fig. 12, the crack initiation zone is marked in red, whereas the intact area is represented in blue. At peak force, the estimated crack initiation lengths at the mid-width are 2.9 mm for HP and 2.5 mm for VB specimens. This difference is attributed to the variation in G_{IIC}, as the simulation methodology remains consistent across both models.

Additionally, a comparative analysis reveals that the onset of damage is marginally greater at the specimen's edge – where plane stress conditions prevail – than at the centreline, which experiences plane strain. This difference arises because plane strain limits material deformation, leading to a narrower plastic region [54]. This behaviour is observed in both HP and VB specimens, as shown in Fig. 12(a)–(b).

6.6. Model validation at difference initial crack lengths

To reinforce the validity of the TTSL, identical parameter values were used to model delamination in VB specimens featuring a_o of 17.5, 22, 26, 33, 37, and 42 mm. Fig. 13 compares the experimental and numerical force-displacement curves for these specimens. The simulation results demonstrate accurate predictions of both the initial stiffness and the maximum force. The largest percentage deviation was observed at a_o = 42 mm, where the difference between experimental and numerical results was approximately 7 % for both the slope and peak force. In the crack growth region, which is represented by the vertical drop in the force, the simulation results closely match the experimental data, except for the case with a_o = 17.5 mm. The numerical force-displacement curve predicts a more pronounced force drop, which is

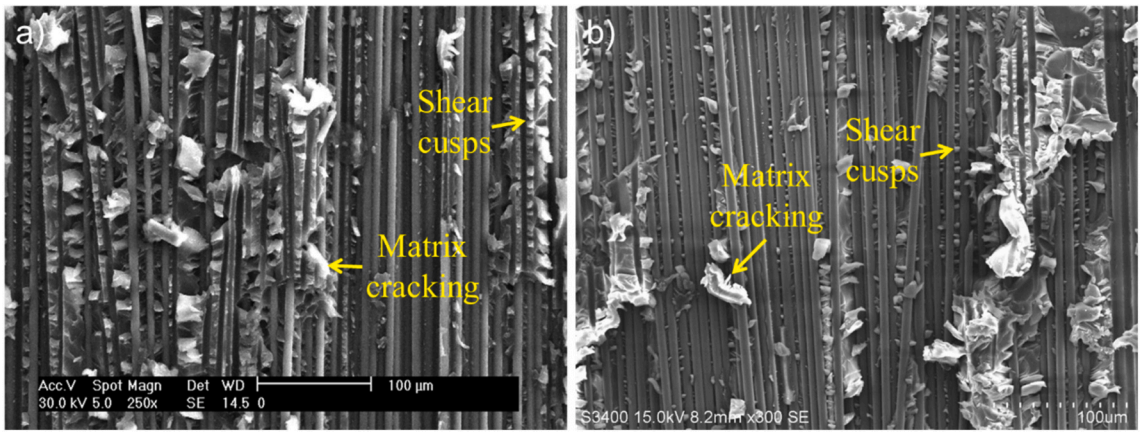

Fig. 9. Scanning electron micrographs of unidirectional carbon/epoxy delamination: (a) hot-press, (b) vacuum-bagging.

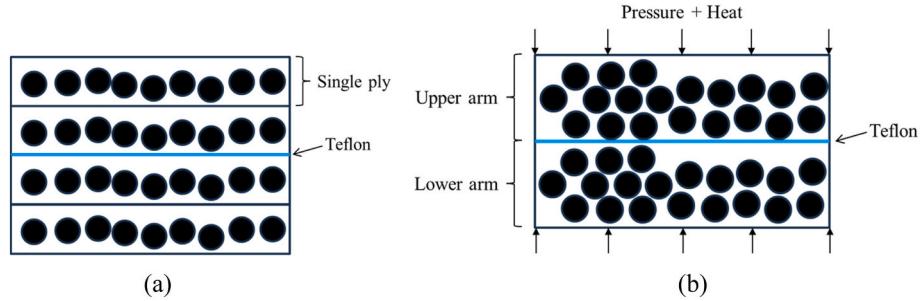

Fig. 10. Schematic illustration of the unidirectional carbon/epoxy composite laminate: (a) before curing (hand-laid prepregs), and (b) after the curing process under applied pressure and temperature.

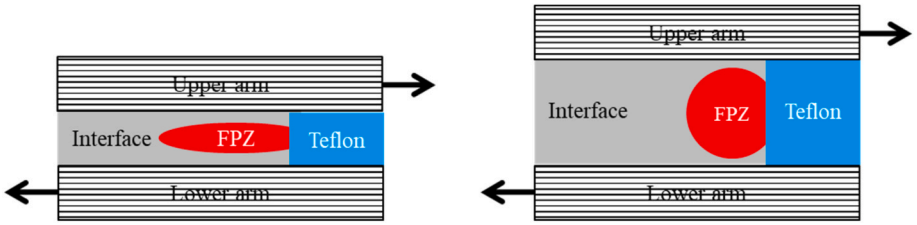

Fig. 11. Schematic illustration of the influence of resin-rich region thickness on the fracture process zone (FPZ) development.

Table 2
Summary of cohesive parameters used in mode II delamination simulations for HP and VB specimens.

Parameter	Hot-press	Vacuum-bagging
G_{IIC}	2.06 N/mm	1.39 N/mm
k_{II}	4.5×10^5 MPa/mm	4.5×10^5 MPa/mm
$t_{u,II}$	100 MPa	100 MPa
Γ	0.99	0.99
$\delta_{o,II}$	2.22×10^{-4} mm	2.22×10^{-4} mm
$\delta_{p,II}$	2.06×10^{-2} mm	1.39×10^{-2} mm
$\delta_{f,II}$	2.08×10^{-2} mm	1.41×10^{-2} mm

consistent with trends observed for other initial crack lengths. Experimentally, however, the data suggest a smaller crack jump in the specimen [42]. This discrepancy may explain why ASTM D7905 recommends an initial crack length of 30 mm for mode II delamination using ENF test [49]. Nevertheless, in this study, specimens with initial crack lengths ranging from 22 mm to 42 mm demonstrated good agreement between experimental and numerical force-displacement responses.

6.7. Further discussion

This study is limited to T600 S/R368-1 unidirectional carbon/epoxy prepregs with a $[0_8//0_8]$ stacking sequence, fabricated using HP and VB techniques. Pure mode II delamination was investigated using the three-point End-Notched Flexure (ENF) test under quasi-static loading at a rate of 1 mm/min. The results of this study establish a unified framework for the numerical simulation of mode II delamination in unidirectional carbon/epoxy composites fabricated using hot-press (HP) and vacuum-bagging (VB) methods. This approach significantly reduces the need for extensive experimental work and parametric studies in numerical simulations. The findings are particularly valuable for predicting shear-induced delamination in composite structures subjected to bending loads, such as aircraft fuselages and stabilisers [38].

Composite components in aircraft are predominantly fabricated using autoclave curing. However, barely visible impact damage (BVID) can occur due to low-energy impact events [55], necessitating structural repair. In many cases, especially in confined spaces, autoclave curing is not feasible for repairs. Under such constraints, vacuum-bagging is a widely adopted alternative, as it allows localised sealing and curing of the repair area. Based on the results of this study, the G_{IIC} of VB

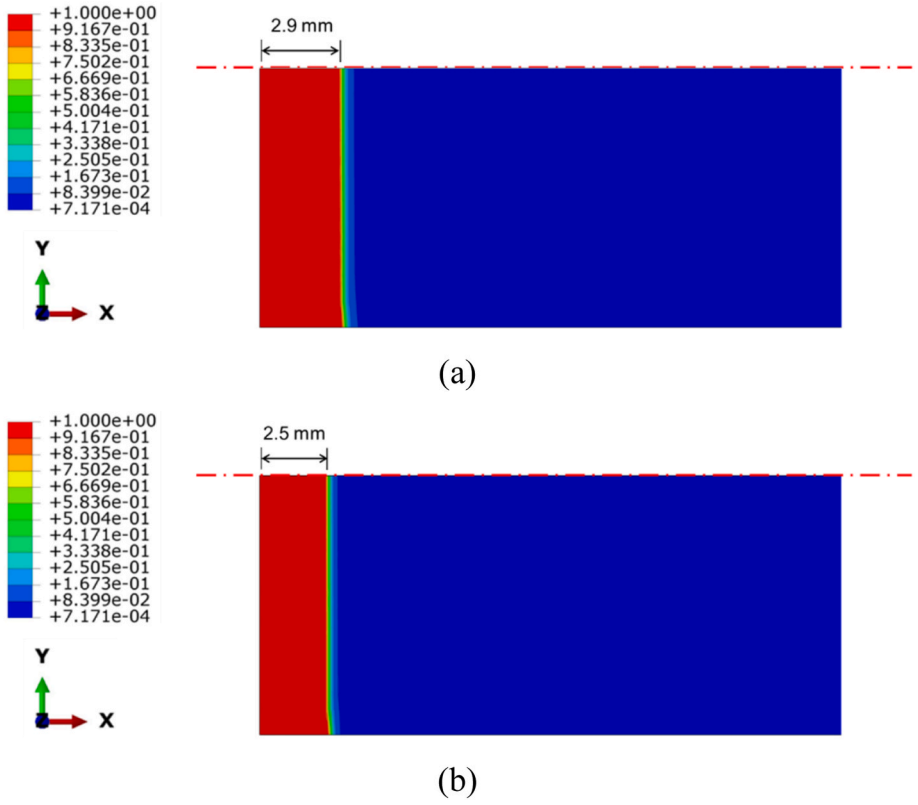

Fig. 12. Damage distribution at peak load for unidirectional carbon/epoxy specimens fabricated via (a) hot-press and (b) vacuum-bagging.

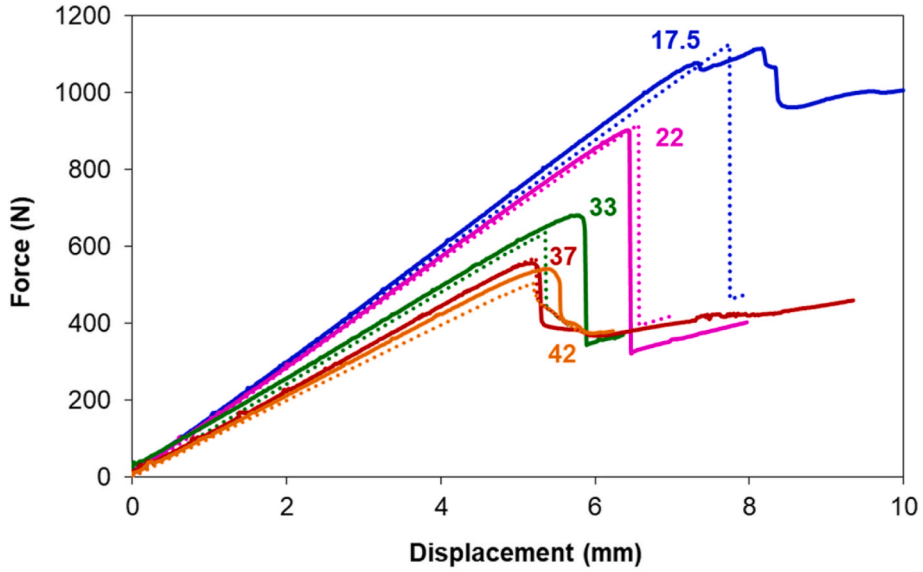

Fig. 13. Comparison of experimental and numerical force-displacement responses for vacuum-bagged specimens with varying initial crack lengths. Solid lines represent experimental data, while dashed lines indicate FE-predicted results.

specimens is approximately 33 % lower than that of HP specimens. This suggests that repaired regions may exhibit reduced resistance to shear-induced delamination, which is commonly triggered under bending loads. Therefore, this reduction in interlaminar toughness should be carefully considered when employing vacuum-bagging techniques for repairing primary composite structures in aircraft.

Given the complexity of real-world composite structures and loading conditions, this work provides a foundation for future studies involving multidirectional laminates and mixed-mode delamination. Furthermore, the proposed numerical simulation methodology holds potential for application to other composite systems, enabling the development of a unified set of cohesive parameters across different material configurations.

7. Conclusions

A validated unified framework for simulating mode II interface delamination process in laminated composites, fabricated by different

techniques has been developed. The mode II interface delamination processes in unidirectional carbon/epoxy composite laminates via hot-press (HP) and vacuum-bagging (VB) techniques through both experimental testing and numerical simulation have been quantified. The key findings are summarised as follows:

i) Force-Displacement Behaviour:

Both HP and VB specimens exhibited similar responses under mode II loading, characterised by a linear increase in force with displacement followed by a sudden drop at peak force, indicating crack propagation.

ii) Fracture Toughness Comparison:

The mode II fracture toughness (G_{IIC}) of VB specimens was measured at 1387.19 N/m, which is approximately 33 % lower than that of HP specimens (2058.27 N/m).

iii) Microscopic Damage Analysis:

Scanning electron micrographs revealed that VB specimens showed less severe damage features, such as fewer shear cusps and matrix cracks, suggesting lower energy dissipation and correlating with the reduced G_{IIC} value.

iv) Numerical Modelling Validation:

The Trapezoidal Traction-Separation Law (TTSL), using consistent parameters – interface stiffness (k_{II}) = 4.5 × 10^5 N/mm, interface strength ($t_{u,II}$) = 100 MPa, and pseudo-plasticity parameter (Γ) = 0.99 – accurately predicted the force-displacement behaviour for both HP and VB specimens. The only variable between models was the experimentally derived G_{IIC} value, confirming the robustness of the cohesive zone modelling approach across different fabrication methods.

v) Damage Profile Analysis:

At peak load, the crack initiation lengths were estimated to be 2.9 mm for HP and 2.5 mm for VB specimens. This difference is attributed to the variation in G_{IIC} values. Additionally, the damage initiation size was slightly larger at the specimen edge (plane stress condition) compared to the mid-width (plane strain condition), due to the constraint in material deformation under plane strain.

CRediT authorship contribution statement

K.J. Wong: Writing – review & editing, Writing – original draft, Visualization, Validation, Supervision, Software, Resources, Project administration, Methodology, Investigation, Funding acquisition, Formal analysis, Data curation, Conceptualization. **H.A. Israr:** Writing – review & editing, Visualization, Validation, Methodology, Formal analysis, Conceptualization. **T. Dickhut:** Writing – review & editing, Visualization, Validation, Project administration, Methodology, Funding acquisition, Formal analysis. **S.S.R. Koloor:** Writing – review & editing, Visualization, Validation, Resources, Project administration, Methodology, Funding acquisition, Formal analysis. **M.N. Tamin:** Writing – review & editing, Visualization, Validation, Supervision, Resources, Project administration, Methodology, Funding acquisition, Formal analysis, Conceptualization.

Declaration of competing interest

The authors declare that they have no known competing financial interests or personal relationships that could have appeared to influence the work reported in this paper.

Acknowledgements

The authors highly acknowledge the financial support from the Ministry of Higher Education under Fundamental Research Grant Scheme, UTM, FRGS/1/2022/TK10/UTM/02/27 (R. J130000.7851.5F517). Also, the authors appreciate the support of Chair of Composite Materials and Technical Mechanics, Faculty of Mechanical Engineering, Universität der Bundeswehr München (UniBW) through the project “Development of Concept and Materials for a Space-adapted Hydrogen Tank for Efficient Integration in Aircraft”, under the guidance of German Aerospace Center (DLR), which is financed by the “Bundesministeriums für Wirtschaft und Klimaschutz” - registration number 20E2204C. The financial support by Universitä t der Bundeswehr München for Open Access publication is also acknowledged.

Data availability

Data will be made available on request.

References

[1] V.M. Drakonakis, J.C. Seferis, C.C. Doumanidis, Curing pressure influence of out-of-autoclave processing on structural composites for commercial aviation, Adv. Mater. Sci. Eng. 2013 (1) (2013) 356824.
[2] F. Elaldi, An experimental study on rapid composite repair techniques, in: 15th European Conference on Composite Materials, 2012. Venice, Italy.
[3] T. Centea, L.K. Grunenfelder, S.R. Nutt, A review of out-of-autoclave prepregs – material properties, process phenomena, and manufacturing considerations, Compos. Appl. Sci. Manuf. 70 (2015) 132–154.
[4] J.K. Sutter, W.S. Kenner, L.I. Pelham, S.G. Miller, D.L. Polis, C.L. Nailadi, T.J. E. Zimmerman, R.D. Lort, T.H. Hou, D.J. Quade, B.A. Lerch, J. Walker, J.C. Fikes, Comparison of autoclave and out-of-autoclave composites, in: SAMPE 2010 Technical Conference, 2010. Salt Lake City, UT.
[5] B. Dewangan, N.D. Chakladar, Influence of out-of-autoclave and autoclave manufacturing processes on mechanical properties of glass fiber-reinforced epoxy composite, Polym. Compos. 45 (17) (2024) 15998–16020.
[6] K. Abdurohman, R.A. Pratomo, R. Hidayat, R.A. Ramadhan, T.S. Nurtiasto, R. Ardiansyah, M.G.P.P. Pratama, A comparison of vacuum infusion, vacuum bagging, and hand Lay-Up process on the compressive and shear properties of GFRP materials, Indonesian Journal of Aerospace 21 (1) (2023) 39–50.
[7] B. Abdi, S. Koloor, M. Abdullah, A. Amran, M.Y. Yahya, Effect of strain-rate on flexural behavior of composite sandwich panel, Appl. Mech. Mater. 229 (2012) 766–770.
[8] A. Turon, P.P. Camanho, J. Costa, J. Renart, Accurate simulation of delamination growth under mixed-mode loading using cohesive elements: definition of interlaminar strengths and elastic stiffness, Compos. Struct. 92 (8) (2010) 1857–1864.
[9] K.O. Low, M. Johar, A.N. Sung, M.N.M. Nasir, S.S.R. Koloor, M. Petrů, H.A. Israr, K. J. Wong, Displacement rate effects on mixed-mode I/II delamination of laminated carbon/epoxy composites, Polym. Test. 108 (2022) 107512.
[10] K.J. Wong, M. Johar, S.S.R. Koloor, M. Petrů, M.N. Tamin, Moisture absorption effects on mode II delamination of carbon/epoxy composites, Polymers 12 (9) (2020) 2162.
[11] X.T. Chia, W.W.F. Chong, A.B. Chai, K.J. Wong, Mode I delamination of unidirectional carbon/epoxy composites by different fabrication methods: experiments and cohesive zone modeling, Mech. Adv. Mater. Struct. (2025).
[12] S. Koloor, A. Abdul-Latif, M.N. Tamin, Mechanics of composite delamination under flexural loading, Key Eng. Mater. 462 (2011) 726–731.
[13] M. Joshani, S. Koloor, R. Abdullah, Damage mechanics model for fracture process of steel-concrete composite slabs, Appl. Mech. Mater. 165 (2012) 339–345.
[14] J. Zhang, J. Wang, Z. Yuan, H. Jia, Effect of the cohesive law shape on the modelling of adhesive joints bonded with brittle and ductile adhesives, Int. J. Adhesion Adhes. 85 (2018) 37–43.
[15] Y. Xu, Y. Guo, L. Liang, Y. Liu, X. Wang, A unified cohesive zone model for simulating adhesive failure of composite structures and its parameter identification, Compos. Struct. 182 (2017) 555–565.
[16] R.D.S.G. Campilho, M.D. Banea, J.A.B.P. Neto, L.F.M. da Silva, Modelling adhesive joints with cohesive zone models: effect of the cohesive law shape of the adhesive layer, Int. J. Adhesion Adhes. 44 (2013) 48–56.
[17] F.J.P. Chaves, L.F.M. da Silva, M.F.S.F. de Moura, D.A. Dillard, V.H.C. Esteves, Fracture mechanics tests in adhesively bonded joints: a literature review, J. Adhes. 90 (12) (2014) 955–992.
[18] R.D.F. Moreira, M. de Moura, R.J.B. Rocha, C.F.M. Oliveira, Mode II fracture characterisation of a honeycomb/carbon-epoxy sandwich panel using the asymmetric end-notched flexure test, J. Sandw. Struct. Mater. 24 (7) (2022) 2030–2046.
[19] A.S.M. Al-Azzawi, L.F. Kawashita, C.A. Featherston, Predicting interlaminar damage behaviour of fibre-metal laminates containing adhesive joints under bending loads, J. Reinforc. Plast. Compos. 41 (5–6) (2021) 167–186.

[20] A.S.M. Al-Azzawi, L.F. Kawashita, C.A. Featherston, A modified cohesive zone model for fatigue delamination in adhesive joints: numerical and experimental investigations, Compos. Struct. 225 (2019) 111114.
[21] M. Noruzi, H. Khoramishad, An equivalent cohesive zone model for a wide range of ductile and brittle adhesives, Fatig. Fract. Eng. Mater. Struct. 46 (10) (2023) 3939–3952.
[22] M.F.S.F. de Moura, J.P.M. Gonçalves, J.A.G. Chousal, R.D.S.G. Campilho, Cohesive and continuum mixed-mode damage models applied to the simulation of the mechanical behaviour of bonded joints, Int. J. Adhesion Adhes. 28 (8) (2008) 419–426.
[23] M. May, H. Voß, S. Hiermaier, Predictive modeling of damage and failure in adhesively bonded metallic joints using cohesive interface elements, Int. J. Adhesion Adhes. 49 (2014) 7–17.
[24] K.N. Anyfantis, N.G. Tsouvalis, Experimental and numerical investigation of mode II fracture in fibrous reinforced composites, J. Reinforc. Plast. Compos. 30 (6) (2011) 473–487.
[25] M. Tauheed, N.V. Datla, Characterization and prediction of hygrothermally aged CFRP adhesive joint subjected to mode II load, Composites Part C: Open Access 11 (2023) 100357.
[26] P. Ghabezi, M. Farahani, Trapezoidal traction–separation laws in mode II fracture in nano-composite and nano-adhesive joints, J. Reinforc. Plast. Compos. 37 (11) (2018) 780–794.
[27] M.N. Mohd Fua'ad, K.J. Wong, H.A. Israr, T. Dickhut, S.S.R. Koloor, A new cohesive-based modelling of moisture-dependent mode II delamination of carbon/epoxy composites, J. Mater. Res. Technol. 32 (2024) 817–826.
[28] M. Johar, W.W.F. Chong, H.S. Kang, K.J. Wong, Effects of moisture absorption on the different modes of carbon/epoxy composites delamination, Polym. Degrad. Stabil. 165 (2019) 117–125.
[29] M. Johar, K.O. Low, H.A. Israr, K.J. Wong, Mode I and mode II delamination of a chopped strand mat E-glass reinforced vinyl ester composite, Plast, Rubber Compos. 47 (9) (2018) 391–397.
[30] T.S. Rajendran, M. Johar, K.O. Low, S. Abu Hassan, K.J. Wong, Interlaminar fracture toughness of a plain weave flax/epoxy composite, Plast, Rubber Compos. 48 (2) (2019) 74–81.
[31] P. Naghipour, M. Bartsch, L. Chernova, J. Hausmann, H. Voggenreiter, Effect of fiber angle orientation and stacking sequence on mixed mode fracture toughness of carbon fiber reinforced plastics: numerical and experimental investigations, Mater. Sci. Eng., A 527 (3) (2010) 509–517.
[32] P. Naghipour, J. Schneider, M. Bartsch, J. Hausmann, H. Voggenreiter, Fracture simulation of CFRP laminates in mixed mode bending, Eng. Fract. Mech. 76 (18) (2009) 2821–2833.
[33] H. Senol, H. Ulus, A. Al-Nadhari, S. Topal, M. Yildiz, Ameliorating tensile and fracture performance of carbon fiber-epoxy composites via atmospheric plasma activation: insights into damage modes through in-situ acoustic emission inspection, Compos. Appl. Sci. Manuf. 195 (2025) 108929.
[34] Y. Zhao, W. Liu, L.K. Seah, G.B. Chai, Delamination growth behavior of a woven E-glass/bismaleimide composite in seawater environment, Compos. B Eng. 106 (2016) 332–343.
[35] L.R. LeBlanc, G. LaPlante, Experimental investigation and finite element modeling of mixed-mode delamination in a moisture-exposed carbon/epoxy composite, Compos. Appl. Sci. Manuf. 81 (2016) 202–213.
[36] R. Mohammadi, R. Akrami, M. Assaad, A. Imran, M. Fotouhi, Comparative analysis of delamination resistance in CFRP laminates interleaved by thermoplastic nanoparticle: evaluating toughening mechanisms in modes I and II, Composites Part C: Open Access 15 (2024) 100518.
[37] H. Senol, H. Ulus, C. Yildirim, A. Al-Nadhari, S. Topal, M. Yildiz, Assessing fracture toughness performance of adhesively bonded carbon fiber/epoxy composite joints accompanied by acoustic emission inspection: effect of surface treatment methods, Eng. Fract. Mech. 321 (2025) 111119.
[38] C. Yildirim, H. Ulus, H.S. Sas, M. Yildiz, Evaluating the influence of service conditions on the out-of-plane and in-plane loading performance and damage behavior of unidirectional CF/PEKK composites for aerospace applications, Compos. B Eng. 304 (2025) 112637.
[39] M. Johar, H.A. Israr, K.O. Low, K.J. Wong, Numerical simulation methodology for mode II delamination of quasi-isotropic quasi-homogeneous composite laminates, J. Compos. Mater. 51 (28) (2017) 3955–3968.
[40] K.J. Wong, M. Johar, S.S. Koloor, M. Petrů, M.N. Tamin, Moisture absorption effects on mode II delamination of carbon/epoxy composites, Polymers 12 (9) (2020).
[41] K.O. Low, M. Johar, H.A. Israr, K.W. Gan, S.S. Rahimian Koloor, M. Petrů, K. J. Wong, Displacement rate effects on the mode II shear delamination behavior of carbon fiber/epoxy composites, Polymers 13 (11) (2021).
[42] S.S.R. Koloor, M.N. Tamin, Mode-II interlaminar fracture and crack-jump phenomenon in CFRP composite laminate materials, Compos. Struct. 204 (2018) 594–606.
[43] T. Kusaka, T. Kurokawa, M. Hojo, S. Ochiai, Evaluation of mode II interlaminar fracture toughness of composite laminates under impact loading, Key Eng. Mater. 141–143 (1997) 477–500.
[44] A. Laksimi, A. Ahmed Benyahia, X.L. Gong, S. Benmedakhene, Mode II delamination in ± laminates: analysis and optimisation, Adv. Compos. Mater. 9 (3) (2000) 207–221.
[45] A.B. de Morais, Novel cohesive beam model for the end-notched flexure (ENF) specimen, Eng. Fract. Mech. 78 (17) (2011) 3017–3029.
[46] W. Tu, J.-A. Pascoe, R. Alderliesten, Comparison of mode II delamination behaviours in multidirectional and unidirectional composite laminates, Compos. B Eng. 291 (2025) 111941.
[47] M. Mohammadi, E.M. Sosa, Enhancing mode-II delamination resistance of hybrid woven composite materials of glass/Kevlar fabrics by stitching with kevlar threads, Compos. Struct. 345 (2024) 118365.
[48] G.R. Irwin, J.A. Kies, Critical energy rate analysis of fracture strength, Weld. J.Res. Suppl. 33 (1954) 193–198.
[49] ASTM D7905. Standard Test Method for Determination of the Mode II Interlaminar Fracture Toughness of Unidirectional fiber-reinforced Polymer Matrix Composites, ASTM International, West Conshohocken, Pennsylvania, United States, 2014.
[50] C. Yildirim, H. Ulus, H.S. Sas, S. Topal, M. Yildiz, Assessing the fracture and dynamic mechanical performance of CF/PEKK joints bonded with epoxy-based adhesive film for aerospace applications: impact of thermal and cycling hygrothermal conditions, Compos. Appl. Sci. Manuf. 190 (2025) 108659.
[51] K. Trakas, M.T. Kortschot, The relationship between critical strain energy release rate and fracture mode in multidirectional carbon-fiber/epoxy laminates, in: E. A. Armanios (Ed.), Composite Materials: Fatigue and Fracture - ASTM STP 1285, 1997, pp. 283–304.
[52] C.S. Meyer, E. Bonyi, K. Drake, T. Obafemi-Babatunde, A. Daodu, D. Ajifa, A. Bigio, J. Taylor, B.Z. Haque, D.J. O'Brien, J.W. GillespieJr, K. Aslan, Automated detection and quantification of transverse cracks on woven composites, J. Reinforc. Plast. Compos. 40 (23–24) (2021) 898–911.
[53] M.F.S.F. de Moura, J.A.G. Chousal, Cohesive and continuum damage models applied to fracture characterization of bonded joints, Int. J. Mech. Sci. 48 (5) (2006) 493–503.
[54] T.L. Anderson, Fracture Mechanics: Fundamentals and Applications, CRC press, 2017.
[55] A. Shahdin, L. Mezeix, C. Bouvet, J. Morlier, Y. Gourinat, Monitoring the effects of impact damages on modal parameters in carbon fiber entangled sandwich beams, Eng. Struct. 31 (12) (2009) 2833–2841.